Research in Astronomy and Astrophysics, 23:125007 (9pp), 2023 December https://doi.org/10.1088/1674-4527/acf6b1

A Novel Low-frequency Radio Astronomical Observation Array (1 ∼ 90 MHz) and its First Light

Wen-Jun Yang[1,2,3], Zhen Wang[1,2,3], Ming-Yuan Wang[4,5], Fa-Bao Yan[6], Guang Lu[6], Guan-Nan Gao[2,7], Shao-Jie Guo[2,7], Yu-Mei Shen[5], Bing-Qiang Xu[6], Yu Bai[6], Yong Chen[1,2,3], and Jin-Song Ping[4,5]
[1] Xinjiang Astronomical Observatory, Chinese Academy of Sciences, Urumqi 830011, China; wangzh@xao.ac.cn
[2] Yunnan Key Laboratory of the Solar Physics and Space Science, Kunming 650216, China
[3] Xinjiang Key Laboratory of Radio Astrophysics, Urumqi 830011, China
[4] School of Astronomy and Space Science, University of Chinese Academy of Sciences, Beijing 100049, China; wangmy@nao.cas.cn
[5] National Astronomical Observatories, Chinese Academy of Sciences, Beijing 100101, China
[6] Weihai campus, Shandong University, Weihai 264209, China
[7] Yunnan Observatories, Chinese Academy of Sciences, Kunming 650011, China
Received 2023 May 10; revised 2023 August 25; accepted 2023 August 30; published 2023 October 27

Abstract

The extremely low frequency ($f < 40$ MHz) is a very important frequency band for modern radio astronomy observations. It is also a key frequency band for solar radio bursts, planetary radio bursts, fast radio bursts detected in the lunar space electromagnetic environment, and the Earth's middle and upper atmosphere with low dispersion values. In this frequency band, the solar stellar activity, the early state of the universe, and the radiation characteristics of the planetary magnetosphere and plasma layer can be explored. Since there are few observations with effective spatial resolution in the extremely low frequency, it is highly possible to discover unknown astronomical phenomena on such a band in the future. In conjunction with low frequency radio observation on the far side of the Moon, we initially set up a novel low-frequency radio array in the Qitai station of Xinjiang Astronomical Observatory deep in Tianshan Mountains, Xinjiang, China on 2021 August 23. The array covers an operating frequency range of 1 ∼ 90 MHz with a sensitivity of −78 dBm/125kHz, a dynamic range of 72 dB, and a typical gain value of 6 dBi, which can realize unattended all-weather observations. The two antennas due south of the Qitai Low-Frequency Radio Array were put into trial observations on 2021 May 28, and the very quiet electromagnetic environment of the station has been confirmed. So far, many solar radio bursts and other foreign signals have been detected. The results show that this novel low frequency radio array has the advantages of good performance, strong direction, and high antenna efficiency. It can play a unique role in Solar Cycle 25, and has a potential value in prospective collaborative observation between the Earth and space for extremely low frequency radio astronomy.

Key words: The Sun – Astronomical Instrumentation – Methods and Techniques – Stars – Planetary Systems

1. Introduction

The radio technology in the radio wave band did not really develop until the 1940s. In the late 1940s, many radar systems used for military surveillance were transformed into astronomical telescopes by radio scientists for low-frequency radio observations, especially in Britain, France, and Australia. During this period, ground-based low-frequency radio observations entered a stage of vigorous development (Orchiston & Sullivan 2010; Boonstra et al. 2016). Since 1958, a series of low-frequency radio arrays have been established in Australia (George et al. 2015; Orchiston et al. 2015). Many considerable scientific achievements, such as the discovery of Jupiter's eruptions, the first extremely low-frequency radio contour map of the Milky Way (Cane & Whitham 1977), and uneven topography of the Moon's surface, were yielded using these low-frequency antennas. Especially pulsars, quasars, microwave background radiation, and interstellar organic molecules are known as the four major astronomical discoveries in the 1960s which are all based on radio astronomical observations. These remarkable discoveries laid the foundation for the later development of low-frequency radio astronomy. In the 1990s, many low-frequency radio antennas were capable of making high-resolution observations with targets covering the Earth's magnetosphere, cislunar environment, solar radio, galaxies, quasars, and so on.

Since the 21st century, with the rapid development of science and technology, the speed and ability of computer data processing have been greatly improved, so that various disciplines have made great progress in terms of technology and achievements, and low-frequency radio astronomy has therefore entered an unprecedented stage of rapid developments. There are roughly three methods of low-frequency radio observations, including ground-based low-frequency radio

Table 1
Domestic and Foreign Low-frequency Equipment or Stations and Parameters

Name	Frequency range
LWA (The Long Wavelength Array)	10∼88 MHz
LOFAR (The Low-Frequency Array)	30∼240 MHz
Mingantu observation Station in Inner Mongolia	30∼70 MHz
SKA-low (Square Kilometre Array-low)	50∼350 MHz
21CMA (21 Centimeter Array)	50∼200 MHz
Yunnan Observatories	70∼700 MHz
FAST (Five-hundred-meter Aperture Spherical radio Telescope)	70∼3000 MHz
Chashan Solar Radio Observatory, Shandong University	150∼500 MHz
DSRT (Daocheng Solar Radio Imaging Telescope)	150∼450 MHz

observations, space low-frequency radio observations, and lunar low-frequency radio detections (Mei et al. 2018). On 2019 January 3, Chang 'e-4 satellite, China's equipped with an extremely low-frequency radio spectrometer (Zhang & Su 2019) (operating frequency: 0.1∼40 MHz) successfully made a soft landing on the far side of the Moon, marking a breakthrough in China's lunar base low-frequency radio detection. Considering many factors such as construction periods, maintenance, and operation costs, ground-based low-frequency radio observations are obviously the most economical way, compared with space and lunar low-frequency radio observations. However, due to the existence of a natural high-pass filter—Earth's ionosphere, the meter-wave (10∼40 MHz) signals reaching the Earth's surface are seriously distorted. The cut-off frequency (10 MHz) of the ionosphere depends on the characteristics of the ionosphere. The lower the degree of ionization in the atmosphere, the easier it is for electromagnetic waves to reach the Earth. To obtain effective data, ground-based low-frequency radio telescopes must avoid the influence of the ionosphere, so the location of the telescope becomes one of the most important factors affecting extremely low-frequency radio observations (George et al. 2015). The lowest degree of ionospheric ionization is in the mid-latitude region at a certain distance from the geomagnetic pole, that is, the ionospheric hole region-ionospheric trough (He et al. 2011). These areas are relatively ideal areas for extremely low-frequency radio observations. In addition, it is also possible to expand the size of the interference array, seek international cooperation, and combine ground-based low-frequency radio antennas, space satellites, and lunar low-frequency radio scientific observation equipment for joint observation, so as to achieve detection effect with lower frequency, higher sensitivity and higher resolution. Table 1 lists domestic and foreign representative low-frequency instruments (or stations) and their parameters (Ellingson et al. 2009; van Haarlem et al. 2013; Han et al. 2016; Peng et al. 2017; Chen et al. 2021; Dong 2022; Lu et al. 2022; Xu 2022; Zhao et al. 2022).

The remaining part of this paper is organized as follows: In Section 2, we mainly introduce the site selection, and construction of the Qitai Low-Frequency Radio Array (Qitai LFRA), the basic working principle of observation system and relevant tests of the low-frequency radio array; In Section 3, we present the debugging of the system, and show the observation results of solar radio bursts captured by the array, and the last section gives the conclusion and expectation of this paper.

2. Qitai LFRA

2.1. The Site Selection and Construction

Meteorological conditions, radio environment, geographical location, geological features, and basic conditions (roads, water, electricity, communications), etc. are all key considerations for radio telescope siting (Wang 2014). Qitai station is located at the northern foot of the Tianshan Mountains, about 260 kilometers from Urumqi. It is located in a basin about 1.5 kilometers long from east to west and 2 kilometers long from north to south, with an altitude of 1730 ∼ 1830 m. The station is surrounded by mountain ridges at an altitude of approximately 1900 m, providing an enclosed environment that helps reduce radio frequency interference. In addition, Qitai station is also the location of the 110-meter-aperture radio telescope (Qitai Radio Telescope, QTT) under construction.

By referring to the site selection data of QTT, it can be seen that Qitai station is a basin with a high in the southeast and a low in the northwest, with good sealing and good isolation from surrounding areas. Peripheral radio applications mainly include mobile wireless communication (UHF, L, S band), broadcast television (analog and digital) (VHF, UHF band), and satellite TV wireless differential systems (UHF, C band) (Wang 2014). The radio interference detected by the automatic radio environment measurement system (Monitoring frequency: 80 MHz∼12 GHz) for the QTT site is mainly concentrated in the 410 ∼ 1000 MHz frequency band (Liu 2017; Liu et al. 2019). In addition, the Qitai station's basic conditions, geological and meteorological conditions also fully meet the site selection requirements. Generally speaking, Qitai station is far away from the city, and the terrain of the basin has a certain impact on electromagnetic shielding, which is conducive to long-term radio environmental protection. It is an excellent place for astronomical observation, as shown in Figure 1.

After the field investigation of Qitai station, the construction site of Qitai LFRA was finally determined to be about 100 m south of the wind tower in the park, its geographical position is 43°36′ north latitude and 89°41′ east longitude, which is a mid-latitude area with an altitude of 1,675.90 m, as shown in Figure 2. Construction of Qitai LFRA began in 2020 October and was initially completed on 2021 August 23. The construction work mainly includes antenna pier processing, equipment room production, power supply cable laying,

Figure 1. The aerial view of Qitai station.

Figure 2. The construction site of Qitai LFRA (The wind tower direction is due north).

antenna main erection, antenna array installation, etc. We have monitored the nearby radio environment (Test frequency band: 1∼60 MHz) with the log-periodic antenna that has been built, it was found that the signal frequency of the interference band in this area is mainly concentrated below 20 MHz, and the signal frequency band above 20 MHz is relatively clean. The power of interference signal is roughly $-50 \sim -60$ dBm/15 kHz, the power of 11.6 MHz can reach -47 dBm/15 kHz, and the power of signal above 20 MHz is roughly $-110 \sim -120$ dBm/15 kHz, the difference between the two is about 60 dB, overall consideration, we will focus on the detection target above 20 MHz in the future. The monitoring results are shown in Table 2.

Table 2
Main Radio Interference Points and Power near Qitai LFRA

Interference frequency (MHz)	Power (dBm)	Interference frequency (MHz)	Power (dBm)
4.0	−73	15.6	−64
4.9	−67	16.4	−68
5.8	−53	18.4	−89
10.1	−56	27.8	−108
11.6	−47	36.5	−118
13.5	−64	45.1	−120
14.0	−53	58.0	−119

2.2. Antenna Introduction

The antenna (design frequency: 1∼90 MHz) is designed and processed in accordance with medium gain. Due to financial reasons, the corresponding receiver (observation frequency: 1∼62 MHz) is mainly used to receive solar radio signals in the first stage, and the subsequent will cover all bands. For the medium and low gain parts, our observation frequency target will be ∼210 MHz in the future. Qitai LFRA consists of eight antennas. Its main function is to capture, select frequency, and amplify signals. The structure of the antenna is a log-periodic antenna, which is a kind of non-variable frequency antenna with a wide frequency band, simple structure, and lightweight (He & Zhang 2021). In Figure 3, the black block represents the antenna base pier, an antenna is mounted on every three base piers, and there are 24 base piers in total. The column on the base pier is used to support the antenna, and there is a mounting plate between the column and the antenna main rod, which is connected and secured by screws. All the antennas are distributed in a circle with a radius of 11 m. The antennas in the due-south direction are labeled as No.1 and No.2, and the antennas in other directions are labeled in this way, and so on.

The main scientific object of Qitai LFRA is monitoring the radio emission of the Sun and planets in the solar system. Since then the angle between the direction of LFRA and the horizontal plane must be precise to ensure our objects are in the main beam of the antenna. Qitai LFRA also has the task of observing the electromagnetic signals of other stars. For this purpose, eight different pointing antennas have been arranged to expand the observation range of the antennas and cover the entire sky. Qitai LFRA is located on the ridge, the north–south terrain is wide and flat, and the east–west terrain is narrow and sloping. Considering the terrain characteristics and scientific observation targets mainly concentrated in the north–south direction, the eight antennas are arranged on a circular plane at a certain angle, as shown on the left side of Figure 3. In addition, according to scientific research needs, any two adjacent antennas can be selected to simultaneously detect celestial bodies. This shows that Qitai LFRA has certain flexibility in application. The specific performance indicators of each antenna are shown in Table 3. Antennas 1 and 2 are mainly used for coordinated observation with the Chang'e-4 low-frequency radio antenna on the far side of the moon (Ji et al. 2017). Figure 4 is the site map of Qitai LFRA, in which

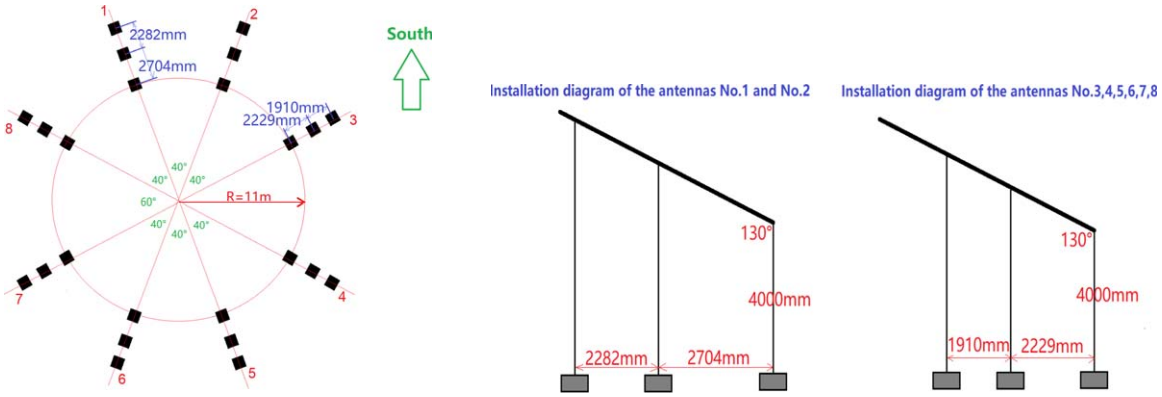

Figure 3. Installation diagram of the antennas.

Table 3
Main Technical Specifications of Antenna

Name	Parameter (The antennas No.1 and No.2)	Parameter (The antennas No.3 to No.8)
Frequency range	15∼70 MHz (Optimum Working Frequency, OWF)	10∼210 MHz (OWF)
Polarization	Horizontal and Vertical	Horizontal and Vertical
Gain	15∼20 MHz: 1.8∼3.0 dBi 25∼40 MHz: 3.0∼6.0 dBi 40∼70 MHz: $\geqslant$ 6.0 dBi	10∼20 MHz: 1.5∼3.0 dBi 20∼35 MHz: 3.0∼7.0 dBi 35∼210 MHz: $\geqslant$ 7.0 dBi
Voltage Standing Wave Ratio (VSWR)	$\leqslant$2.0	$\leqslant$2.0
Angular width (3dB)	81.3 deg.	81.3 deg.
Front-to-back ratio	$\geqslant$ 15 dB	$\geqslant$ 15 dB
Input impedance	50 Ω	50 Ω
Antenna size	6500 mm * 6950 mm	6830 mm * 7500 mm
Wind resistance	60 m s^{-1}	60 m s^{-1}

the white house is the machine room, and the direction of the highest wind tower is due north.

2.3. The S11 Parameter Measurement of the Antenna

A portable vector network analyzer (NanoVNA V2) is a popular tool for measuring antenna parameters. It can measure the S11 parameter, which represents the reflection coefficient of the antenna. Figure 5 is the measurement result of the S11 parameter of antenna 1, and the red curve is the measurement result of the return loss, which measures the amount of power reflected back by the antenna. The blue curve represents the results of a standing wave ratio (SWR) measurement, which measures how well the antenna matches the impedance of the transmission line to which it is connected. The horizontal coordinates represent the measured frequency range (10∼90 MHz). The left side of the ordinate is the return loss (dB), and the right side is the SWR. In the field measurement, the external signal received by the antenna will have a certain influence on the measurement result, which will cause a certain error between the actual measurement result of the antenna and

Figure 4. The scene of Qitai LFRA.

the theoretical measurement result. It can be seen from the figure that the standing wave measurement effect of the antenna below 20 MHz is poor, which may be caused by external interference signals.

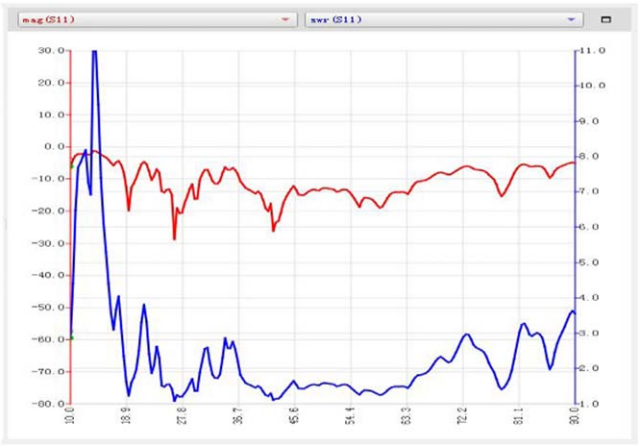

Figure 5. The S11 graph of antenna 1.

Table 4
The Main Performance Parameters of the Observation System

Technical index	Performance parameter
Time Resolution	0.5, 2, 4, 8, 32 ms, default: 4 ms
Frequency Resolution	15.3 kHz
Dynamic Range	72 dB
Noise Figure	-139 dBm Hz^{-1}
Sampling Rate	125 MSPS
Sampling Bit	16 bit

2.4. Observation System

The observation system has a sensitivity of -78 dBm/125 kHz, a maximum signal power amplitude of -6 dBm, and a dynamic range of 72 dB. It includes two groups of log-periodic antennas, corresponding front-end filter and amplification module of analog signal, ADC (Analog-to-Digital Converter) acquisition card, digital signal processing module, upper computer processing and display, data storage and so on (Xu et al. 2023), as shown in Figure 6.

The working principle of the system is described as follows: The antennas receive low-frequency signals from the sky. After initial amplification and frequency selection, the signals are wired into the analog front end through the cable. The analog front end first combines the four channels into two signals, then amplifies and filters the singles, and finally outputs the signals with appropriate frequency and power that can be collected by ADC. After receiving these signals, the acquisition card performs digital signal processing, the FPGA (Field-Programmable Gate Array) processes the signals in real time, and then encapsulates and stores the data. The upper computer can complete the switching between frequency domain and time domain, the selection of accumulation times, the selection of clock source, the selection of drawing and storage path, and so on. The GNSS (Global Navigation Satellite System) antennas pick up satellite signals and feed them to the rubidium clock, which synchronizes time and provides time stamps to the digital signal processing unit. If the amount of data is large, the disk array server can be used to store the data. In addition, remote control and data file transmission can be achieved through the Internet network. The main performance parameters of the observation system are shown in Table 4.

2.5. Observation Equipment

The observation equipment is located in a simple 18-square-meter room, and consists of a regulated power supply, an analog front end, an ADC acquisition and digital signal processing unit, a rubidium clock, a disk array, a network switch, and a GNSS time-frequency receiver, as shown in Figure 7. A Rubidium atomic clock is used to provide time-frequency reference and synchronous time information after training. The disk arrays store observation data transmitted from digital terminals through high-speed optical fibers in real time. After all observation equipment starts running, no observers are required to be on duty, and the remote login can be used for monitoring and debugging. In addition, observers will come to the station regularly to back up observation data, as well as to overhaul and maintain equipment.

3. System Debugging and Observation Data Results

3.1. System Debugging and Trial Observation

The two antennas due south of Qitai LFRA officially entered the system debugging and trial observation operation stage on 2021 May 28. It is found that the 16 bit ADC had collected and recorded signals with a large dynamic range, however, the system also received many interference signals in addition to the local fixed broadcast signals during the trial observation phase. As shown in Figure 8, the left picture and the right picture are for Channel 1 (vertical polarization) and Channel 2 (horizontal polarization), respectively.

Finally, by removing the first stage analog amplifier in Channel 2 (30 dB) and adding a high-pass filter ($\sim$25 MHz) in Channel 1, most of the interference signals were eliminated, and a very clean background signal was obtained (see Figure 9). In the subsequent observations, we can see that these attempts are very effective. After adjustment, Channel 1 has a higher sensitivity detection capability for signals above 20 MHz, and Channel 2 retains detection capability for high-power signals as low as 1 MHz.

3.2. Event Example

At around 08:34:10UT on 2021 July 16, one solar radio burst (Wang et al. 2024) event was detected by Qitai LFRA with a frequency coverage range of 10$\sim$62 MHz for the first

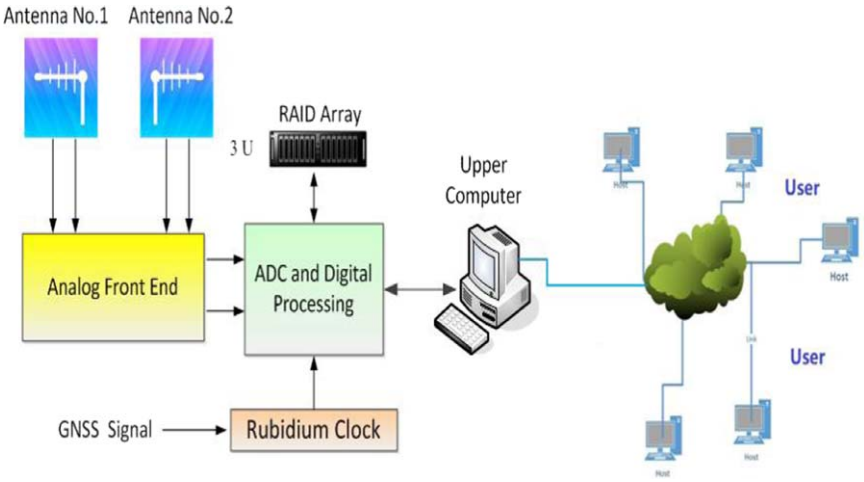

Figure 6. System block diagram.

Figure 7. Observation equipment site.

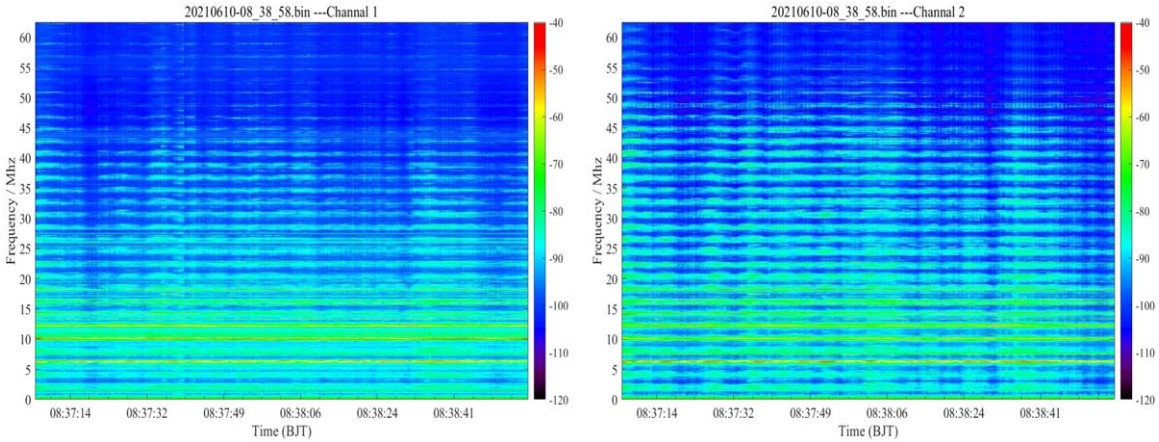

Figure 8. Background signal diagram with more interference in Channel 1 and Channel 2.

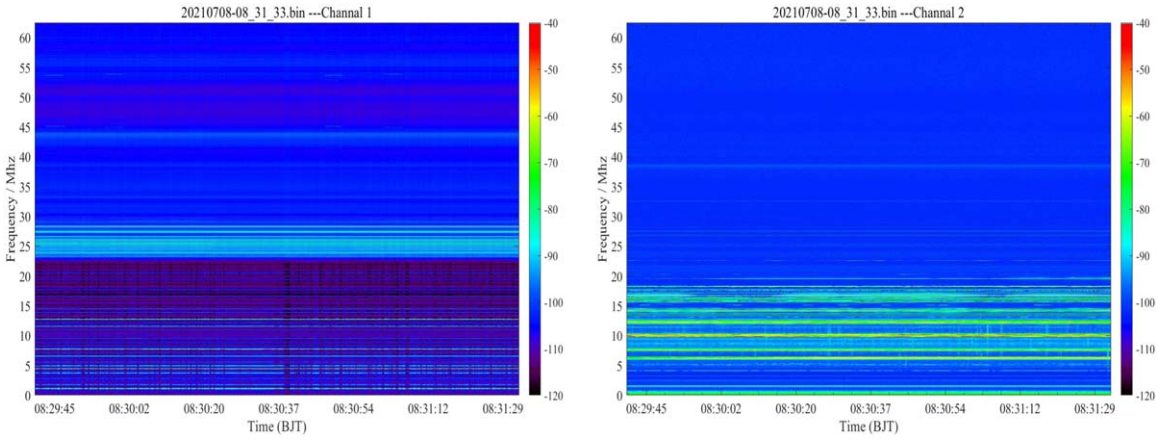

Figure 9. Background signal diagram with less interference in Channel 1 and Channel 2.

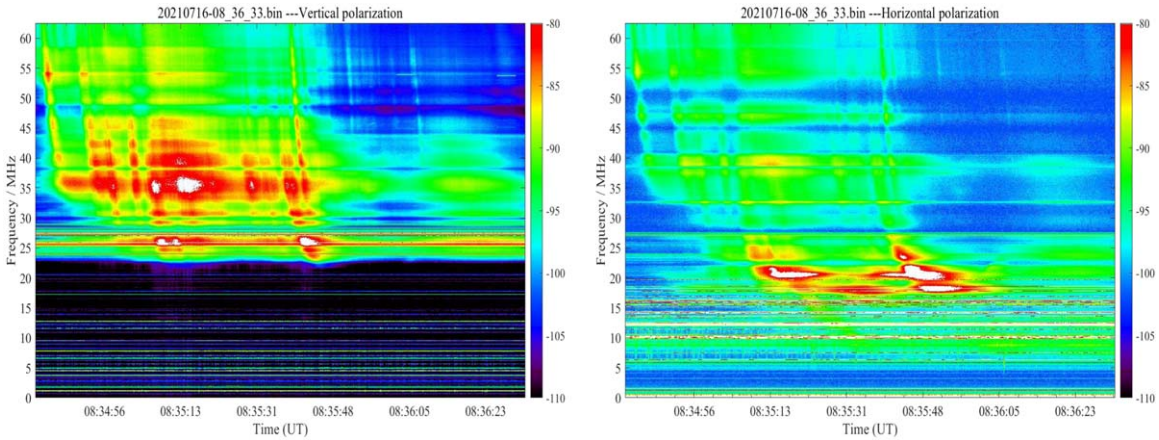

Figure 10. One type III solar burst was detected by Qitai LFRA at around 08:34UT on 2021 July 16. The left is vertical polarization and the right is horizontal polarization with a frequency resolution of 15.3 kHz and a time resolution of 4 ms.

time and a duration of about 2 minutes. This radio burst is consistent with the basic feature of type III solar radio bursts—rapid frequency drift phenomenon, and there is a certain fine structure inside it, and has the J-type characteristics of a type III radio burst, as shown in Figure 10. The fine structure of type III solar radio bursts can be used to diagnose coronal parameters such as electron density, energy electron velocity, and coronal atmospheric turbulence, as well as to predict space weather (Feng & Zhao 2021; Tan et al. 2021). This observed solar radio burst event coincides with the timing of solar X-ray bursts monitored by the National Oceanic and Atmospheric Administration (NOAA), as shown in Figure 11.

At around 06:20UT on 2021 September 28, one type II solar radio burst event was detected by Qitai LFRA for the first time (Yang et al. 2023), which has a frequency coverage range of 18∼50 MHz, a duration of more than 10 minutes, a typical slow frequency drift and band splitting, as shown in Figure 12. According to the preliminary calculation, the frequency drift of the type II radio base frequency structure is about $-0.04\,\mathrm{MHz\,s^{-1}}$. Combined with the Newkirk coronal density model (Smerd et al. 1975), the CME (Coronal Mass Ejection) shock velocity is calculated to be about $500\,\mathrm{km\,s^{-1}}$, which is basically consistent with the CME shock velocity ($524\,\mathrm{km\,s^{-1}}$) detected by SOHO (Solar and Heliospheric Observatory) coronagraph at the same time. In addition, Qitai LFRA still observed the radiation band structure of type II radio bursts at the frequency band with horizontal polarization lower than 25 MHz. This further proves that Qitai LFRA has the ability to detect signals of lower frequencies. At present, Qitai LFRA back-end equipment can only receive signals from two antennas at most, and we will configure new equipment in the later stage to realize scientific observations in the all-sky area.

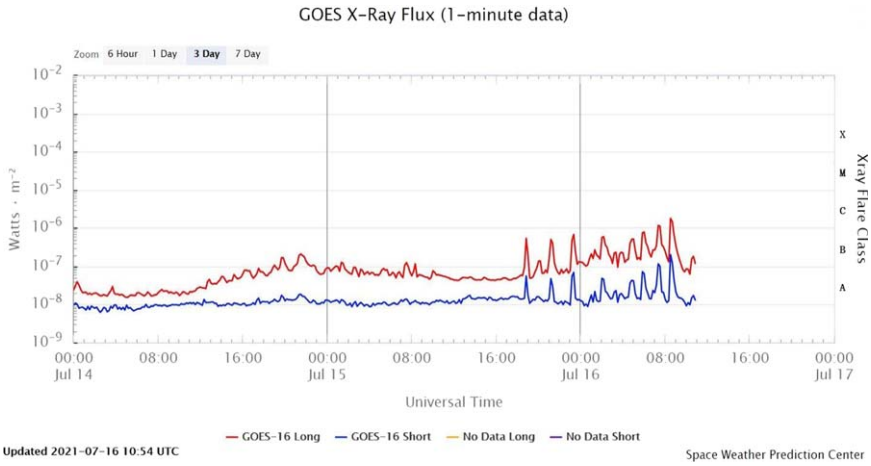

Figure 11. The NOAA's X-ray flow monitor.

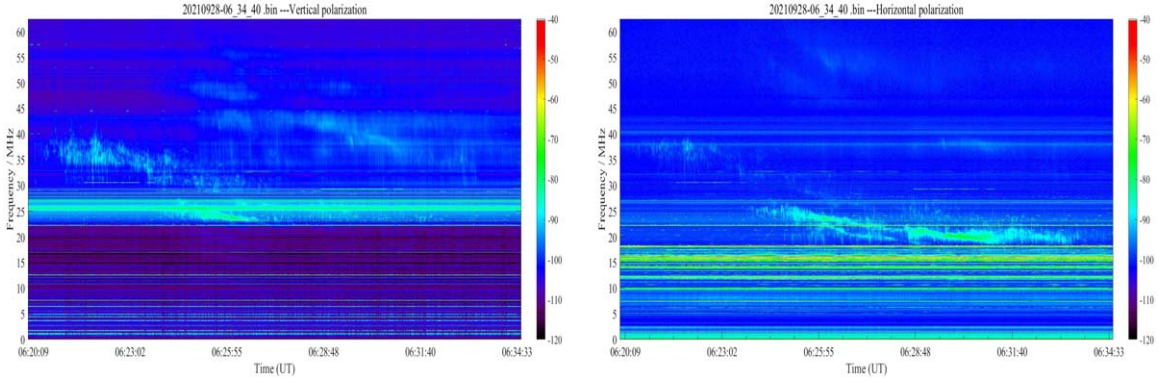

Figure 12. One type II solar burst was detected by Qitai LFRA at around 06:20UT on 2021 September 28. The left is vertical polarization and the right is horizontal polarization with a frequency resolution of 15.3 kHz and a time resolution of 4 ms.

4. Conclusions and Prospects

The development of low-frequency radio astronomy is closely related to the progress of science and technology. With the rapid development of space technology, more and more weak very low-frequency radio signals have been obtained, but ground-based low-frequency radio observations are still a very important and indispensable part. By using all-sky, medium-gain, and synchronous observation techniques, and with the help of interferometry technology similar to remote equipment, we can better suppress artificial noise and extract the radiation signals generated by celestial bodies in this frequency band more sensitively.

It can be seen from the observation results of Qitai LFRA that the array has the characteristics of lower detection frequency, better time resolution and frequency resolution, high sampling accuracy, high sensitivity, large sky coverage area, flexible observation, and so on. It has great advantages in the field of low-frequency radio observation both at home and abroad, especially in the observation range of 1∼40 MHz. In the future, we will consider constructing arrays similar to Qitai LFRA in other areas of Xinjiang, and implementing joint observation by grouping these arrays so as to further improve the observation resolution. We believe that it is very possible to detect unknown astronomical phenomena in this frequency band, and expect to make important scientific discoveries by using the Qitai LFRA platform to fill the gap in the exploration of very low-frequency radio bands.

Acknowledgments

Our work has been supported by "SKA (No.2020SKA0110300)," "Yunnan Key Laboratory of the Solar Physics and Space Science (No.YNSPCC202220)," "The open project of the Key Laboratory in Xinjiang Uygur Autonomous Region of China (No.2023D04058)," the "National Natural Science Foundation of China (No.11941003)," "The Chinese Academy of Sciences Foundation of the young scholars of

western (No.2020-XBQNXZ-019)" and "The 2018 Project of Xinjiang Uygur Autonomous Region of China for Heaven Lake Hundred-Talent Program."

References

Boonstra, A., Garrett, M., Kruithof, G., Wise, M., & Haan, H. 2016, in 2016 IEEE Aerospace Conf. (Piscataway, NJ: IEEE), 1
Cane, H. V., & Whitham, P. S. 1977, MNRAS, 179, 21
Chen, L. J., Yan, Y. H., Fan, Q. X., et al. 2021, RAA, 21, 85
Dong, Z. 2022, Development of Multi-Channel Digital Receiver for Solar Radio Observation in the Meteric-Wavelengh Regime in Chashan Solar Observatory (Shandong: Shandong Univ.)
Ellingson, S. W., Clarke, T. E., Cohen, A. S., et al. 2009, IEEEP, 97, 1421
Feng, S. W., & Zhao, F. 2021, Sci. Sin Tech., 51, 35
George, M., Orchiston, W., Slee, B., et al. 2015, JAHH, 18, 177
George, M., Orchiston, W., Slee, B., et al. 2015, JAHH, 18, 14
Han, Y. B., Tran, V., Tang, L. L., et al. 2016, CJRS, 31, 219
He, M. S., Liu, L. B., Wan, W. X., et al. 2011, JGRD, 116, A05315
He, Y. J., & Zhang, L. 2021, Antenna Technologies (Beijing: Tsinghua Univ.)
Ji, Y. C., Zhao, B., Fang, G. C., et al. 2017, J. Deep Space Explor., 4, 150
Liu, Q., Wang, Y., Liu, Y., et al. 2019, SSPMA, 49, 099512
Liu, Y. 2017, Management Spectrum for Large-aperture Radio Telescope Site (Xinjiang: Xinjiang Univ.)
Lu, G., Wang, B., Chen, Y., et al. 2022, ChJSS, 42, 294
Mei, L., Su, Y., & Zhou, J. F. 2018, AR&T, 15, 127
Orchiston, W., George, M., Slee, B., et al. 2015, JAHH, 18, 3
Orchiston, W., & Sullivan III, W. T. 2010, JAHH, 13, 256
Peng, B., Chai, X. M., Qin, B., et al. 2017, SSPMA, 47, 129501
Smerd, S. F., Sheridan, K. V., & Stewart, R. T. 1975, ApL, 16, 23
Tan, B. L., Huang, J., & Chen, L. J. 2021, J. Deep Space Explor., 8, 92
van Haarlem, M. P., Wise, M. W., Gunst, A. W., et al. 2013, A&A, 556, A2
Wang, N. 2014, SSPMA, 44, 783
Wei, W., Yihua, Y., Baolin, Tan., et al. 2024, Rev. Geophys. Planetary Phys., 55, 1
Xu, B. Q. 2022, Development of $10 \sim 50$ MHz Low Frequency Radio Astronomical Digital Receiver and PC Software (Shandong: Shandong Univ.)
Xu, B. Q., Bai, Y., Lu, G., et al. 2023, ChJG, 66, 891
Yang, W. J., Wang, Z., Ping, J. S., et al. 2023, AR&T, 20, 227
Zhang, T., & Su, Y. 2019, AR&T, 16, 312
Zhao, B. X., Zheng, Q., Shan, H. Y., et al. 2022, RAA, 22, 015012